AD-A169 872

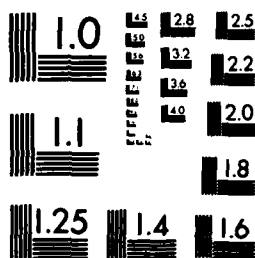NOMOGRAPHIC DESIGN PROCEDURES FOR FIBRE-REINFORCED
METALLIC ROCKET-MOTOR..(U) ROYAL ARMAMENT RESEARCH AND
DEVELOPMENT ESTABLISHMENT FORT HA..  A GROVES ET AL.

1/1

UNCLASSIFIED   JAN 86 RARDE-10/84 DRIC-BR-99277          F/G 21/8     NL

MICROCOPY RESOLUTION TEST CHART

NATIONAL BUREAU OF STANDARDS 1963 A

MINISTRY OF DEFENCE

ROYAL ARMAMENT RESEARCH AND DEVELOPMENT ESTABLISHMENT

REPORT 10/84

Nomographic Design Procedures for Fibre-Reinforced
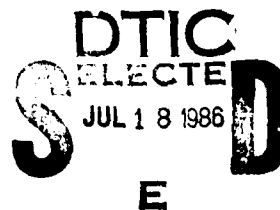
Metallic Rocket-Motor Cases

A Groves
J Margetson
P Stanley*

Summary

Nomographic design procedures are developed for a metallic cylinder (eg a rocket motor case) circumferentially reinforced with a pre-strained fibre overwind with viscoelastic properties. Techniques for calculating the pressure for first yield in the metallic case and the optimum winding conditions for both short- and long- times are presented, together with a technique for determining the maximum fibre stress.

Design examples are presented with each nomogram in turn and the graphical results are compared with exact numerical results.

DTIC
ELECTE
S JUL 1 8 1986
E
D

COPYRIGHT © CONTROLLER HMSO. LONDON 1986

* Simon Engineering Laboratories, University of Manchester

BA/WA/4/1

1

## CONTENTS

| Accession For | |
|---|---|
| NTIS  GRA&I | ☒ |
| DTIC TAB | ☐ |
| Unannounced | ☐ |
| Justification | |
| By | |
| Distribution/ | |
| Availability Codes | |
| Dist | Avail and/or Special |
| A-1 | |

QUALITY INSPECTED 1

## 1    INTRODUCTION

Recent work (Refs 1-4) on the stress states in metallic cylinders circum-
ferentially reinforced with a prestrained fibre overwind has involved analyses
of the initial winding process, the effects of different storage temperatures,
pressurisation and viscoelastic relaxation of the fibre overwind. The
work has particular relevance to the rocket-motor case, and much attention
has been given to the effects of the material and design variables on the
pressure required for the initiation of yield in the reinforced cylinder of
such a case.

The range of choice through the several design variables is considerable,
and it is not easy to assess directly the relative importance of the effects
of changes in these variables. It is in these circumstances that the use
of nomograms for the representation and interpretation of the design
equations offers very considerable advantages, which far outweigh the
small inaccuracies usually associated with graphical solution techniques.

In this report design procedures are developed for the stress analysis of
fibre-reinforced metallic rocket-motor cases. These procedures are pre-
sented graphically in such a way that the effects of changes in the
variables, and their relative importance, can be easily seen. It should
be noted, however, that the procedures presented are general, in that
they may be applied to any fibre-reinforced cylinder subjected to internal
pressure. The effects of the overwind variables (including viscoelastic
relaxation) and pressurisation are taken into account, but thermal effects
have been omitted. Experience has shown that the small changes in the
yield pressure resulting from typical temperature changes do not warrant
the extra complexities in the design charts.

Two of the five nomograms presented are concerned with the determination
of the pressure for the initiation of first yield in the metallic cylinder,
two with an optimisation analysis, and the final nomogram evaluates the
maximum fibre stress. In the last nomogram viscoelastic effects have
been neglected, since numerical results have shown conclusively that the
maximum fibre stress occurs immediately after winding in the outermost
layer.

Design examples are presented with each nomogram. The accuracy of the
solutions are assessed by comparing graphical results with exact numerical
results.

## 2    ELASTIC ANALYSIS

### 2.1    Yield Initiation Predictions

#### 2.1.1    Theory

It is a requirement that the rocket-motor case must withstand all
operational loads without failure or excessive distortion. Although aero-
heat and inertia effects may contribute, the predominant load will always
be the firing pressure. The maximum permissible pressure is defined as
that for the onset of first yield in the metallic case. Although such a

definition does not take into account the strength reserves available in the case after the initiation of yield, this definition will be adopted here.

It has been shown (Ref 3) that for a thin-walled overwound motor case of radius R, overwound with n elastic fibre layers with an initial winding strain $\epsilon_w$ and subjected to the applied firing pressure p, the resulting circumferential stresses in the i'th fibre layer and the case, $\sigma_{\theta fp}^{(i,n)}$ and $\sigma_{\theta cp}^{(n)}$ respectively, are given by

$$\sigma_{\theta fp}^{(i,n)} = \epsilon_w E_f \{1 - AF_i(A,n)\} + \frac{pRA}{t_f(1+An)} \{1 - \frac{\nu_c}{2} (1 - \frac{R_e^2}{R^2})\} ,$$

$$i = 1, 2, \ldots, n \tag{1}$$

and

$$\sigma_{\theta cp}^{(n)} = -E_c \epsilon_w AF_1(A,n) + \frac{pR}{t_c(1+An)} \{1 + \frac{n\nu_c A}{2} (1 - \frac{R_e^2}{R^2})\} ,$$

$$\tag{2}$$

where

$$A = \frac{E_f t_f}{E_c t_c} \tag{3}$$

and

$$F_i(A,n) = \sum_{j=1}^{n} \frac{1}{1+Aj} \tag{4}$$

In the above equations $E_f$ and $E_c$ denote respectively the Young's modulus of the fibre and case, $t_f$ the effective thickness of a single fibre layer and $t_c$ the thickness of the case, $R_e$ the effective nozzle radius (Ref 2) and $\nu_c$ the Poisson's ratio of the case material. The corresponding axial stress component in the case follows from the transverse equilibrium equation, ie

$$\sigma_{zcp} = p \frac{(R^2 - R_e^2)}{2Rt_c} \tag{5}$$

Once the stress components in the metallic case (Eqns 2 and 5) are known, the pressure for the onset of yield can be calculated using the von Mises yield criterion, the most appropriate for the case materials under consideration. If the radial stresses are assumed negligible relative to the circumferential and axial stresses, the yield criterion (Ref 5) reduces to the form

$$(\sigma_{\theta cp}^{(n)})^2 + (\sigma_{zcp})^2 - \sigma_{\theta cp}^{(n)}\sigma_{zcp} = \sigma_y^2 \tag{6}$$

where $\sigma_y$ is the uniaxial yield stress of the case material. Equations 2, 5 and 6 form the basis for nomogram construction.

If used in their present dimensional form, these equations would result in nomograms of unacceptable complexity. However, if the equations are changed into a non-dimensional form the number of variables is reduced and, as a consequence, their graphical representation is considerably simplified.

The following non-dimensional variables are introduced:

$$\beta = An \tag{7}$$

$$\lambda = 1-R_e^2/R^2 \tag{8}$$

$$\hat{p} = p/p_{ymax} = \frac{p\sqrt{3}R\lambda}{4t_c\sigma_y} \tag{9}$$

$$\psi_w = E_c\epsilon_w/\sigma_y \tag{10}$$

$$\hat{\sigma}_{\theta w} = \sigma_{\theta w}/\sigma_y = \psi_w AF_1(A,n) \tag{11}$$

where $\hat{\sigma}_{\theta w}$ is the circumferential case stress due to winding,

$$\hat{\sigma}_{\theta cp}^{(n)} = \sigma_{\theta cp}^{(n)}/\sigma_y \tag{12}$$

$$\hat{\sigma}_{zcp} = \sigma_{zcp}/\sigma_y \tag{13}$$

In Equation 9 the quantity $p_{ymax}$ denotes the maximum attainable yield pressure for the reinforced motor (Ref 2), as given by the equation

$$p_{ymax} = \frac{4t_c\sigma_y}{\sqrt{3}R\lambda} \tag{14}$$

For analytical purposes it is convenient to introduce the approximation

$$AF_1(A,n) + \ln(1+An) \tag{15}$$

so that Equation 11 can be expressed in terms of the variable $\beta$, that is

$$\hat{\sigma}_{\theta w} = \psi_w \ln(1+\beta) \tag{16}$$

With these non-dimensional variables, Equations 2, 5 and 6 can be expressed in non-dimensional form as

$$\hat{\sigma}_{\theta cp}^{(n)} = -\hat{\sigma}_{\theta w} + \frac{2\hat{p}}{\sqrt{3}\lambda(1+\beta)} \{2+ \frac{\beta\lambda}{3}\} \tag{17}$$

$$\hat{\sigma}_{zcp} = \frac{2}{\sqrt{3}} \hat{p} \tag{18}$$

$$(\hat{\sigma}_{\theta cp}^{(n)})^2 + (\hat{\sigma}_{zcp})^2 - \hat{\sigma}_{\theta cp}^{(n)}\hat{\sigma}_{zcp} = 1 \tag{19}$$

where, in Equation 17, it has been assumed that $\nu_c = 1/3$, a typical value for most suitable case materials.

The variables $\beta$ and $\lambda$ are now combined by introducing the auxiliary variable $\phi$, where

$$\phi = \{2+ \frac{\beta\lambda}{3}\}/\{\lambda(1+\beta)\} \tag{20}$$

so that Equation 17 reduces to the four-variable equation

$$\hat{\sigma}_{\theta cp}^{(n)} = -\hat{\sigma}_{\theta w} + \frac{2}{\sqrt{3}} \hat{p}\phi \tag{21}$$

Once the governing equations have been obtained in non-dimensional form (Eqns 18, 19 and 21), in order to predict the pressure for the onset of yield (ie $\hat{p}=\hat{p}_y$) it is necessary to eliminate the quantities $\hat{\sigma}_{\theta cp}^{(n)}$ and $\hat{\sigma}_{zcp}$ from Equation 19 in favour of $\hat{p}_y$ using Equations 21 and 18 respectively, to give the quadratic

$$\hat{p}_y^2 \frac{4}{3}\{1+\phi^2-\phi\} + \hat{p}_y \frac{2}{\sqrt{3}} \{-2\hat{\sigma}_{\theta w}\phi+\hat{\sigma}_{\theta w}\} + \hat{\sigma}_{\theta w}^2 - 1 = 0 \tag{22}$$

Once $\hat{p}_y$ has been obtained, the yield pressure $p_y$ readily follows from Equation 9.

Equation 22 can now be represented graphically by plotting the variation of $\hat{\sigma}_{\theta w}$ with $\phi$ for various $\hat{p}_y$ values, typically from 0 to 1 in increments of 0.1. This is depicted in the central portion of Figure 1.

This graphical technique for evaluating $\hat{p}_y$ is in terms of the variable combinations $\hat{\sigma}_{\theta w}$ and $\phi$. It is now necessary to extend the Equation 22 plot to enable the evaluation of $\hat{p}_y$ to be carried out in terms of the more fundamental variables $\psi_w$, $\beta$ and $\lambda$. From Equation 16 it can be seen that the variable $\hat{\sigma}_{\theta w}$ is a simple multiplication of $\psi_w$ and $\ln(1+\beta)$; this equation can therefore be represented by the 'z' type nomogram (Ref 6) shown to the left of the central plot in Figure 1.

By contrast, the graphical determination of $\phi$ necessitates a rearrangement of the governing Equation 20 so that it complies with an alignment chart (Ref 6) of the form

$$f_1(\lambda) + f_2(\beta)f_3(\phi) = f_4(\beta) \tag{23}$$

where the functions represent

$$f_1(\lambda) = -2/\lambda$$

$$f_2(\beta) = 1 + \beta \tag{24}$$

$$f_3(\phi) = \phi$$

$$f_4(\beta) = \beta/3$$

The Equation 23 nomogram is shown in the lower portion of Figure 1.

The range of the variables associated with these nomograms must be chosen with care to ensure that the final design chart can be used for all practical applications. For fibre-reinforced rocket motor cases these ranges, together with those to be used in subsequent nomograms, are presented in Table 1.

Since the variable $\hat{\sigma}_{\theta w}$ is common to both Equations 16 and 22, and, furthermore, since the variable $\phi$ is common to Equations 20 and 22, it follows that the three nomograms developed can be combined in such a way that the transfer of data from one nomogram to another is, in general, avoided. This reduces reading errors and, omitting constructional details, results in the simple design chart presented in Figure 1.

There are four fundamental variables in the design process embodied in Figure 1, $\psi_w$, $\lambda$, $\hat{p}_y$ and $\beta$. Any one of the first three (ie $\psi_w$ or $\lambda$ or $\hat{p}_y$) can be readily 'read' from the Figure 1 design chart provided the other three are known. However, because the variable $\beta$ is represented in two of the graduated loci in the design chart, it cannot be obtained directly in terms of the variables $\psi_w$, $\lambda$ and $\hat{p}_y$. Nevertheless, a trial-

7

and-error graphical approach for $\beta$ is feasible. The problem is resolved
if $\hat{\sigma}_{\theta w}$ (ie the case stress induced by winding) can be specified together
with $\hat{p}_y$ and $\lambda$; in these circumstances the solution proceeds as follows:

   a.      Determine the $\phi$ value corresponding to the intersection
   of the specified $\hat{\sigma}_{\theta w}$ and $\hat{p}_y$ values in the $\hat{\sigma}_{\theta w}$ - $\phi$ grid depicted
   in the central portion of Figure 1.

   b.      Determine the required $\beta$ value from the Equation 23
   nomogram (lower portion of Fig 1) using the calculated $\phi$ and
   specified $\lambda$ values.

   c.      Obtain $\psi_w$ and thence the winding strain which satisfies
   the prescribed problem using the left-hand side of Figure 1.

## 2.1.2   Graphical Design Example

For the purposes of illustration Figure 1 is used to evaluate the yield
pressure, $p_y$, for a sample motor case (Refs 2&4) in terms of $\psi_w$, $\lambda$ and
$\beta$ (see Tab 3) derived from the details given in Table 2. The design
procedure is as follows:

   a.      Using the left hand side of Figure 1 construct a straight
   line to pass through the derived values of $\psi_w$ = 0.22 and
   $\beta$ = 1.82. Mark the intersection of this line with the $\hat{\sigma}_{\theta w}$
   scale.

   b.      Using the lower right hand portion of the nomogram
   construct a second straight line to pass through $\beta$ =1.82 and
   $\lambda$ = 0.5. Mark the intersection of this line with the $\phi$
   scale.

   c.      Project two lines, the first horizontally and the second
   vertically, across the $\hat{\sigma}_{\theta w}$ - $\phi$ grid from the intersections
   obtained in a. and b. respectively.

   d.      Evaluate the $\hat{p}_y$ value corresponding to the intersection
   of the line drawn in c. and then $p_y$ from Equation 9.

For the example considered, Figure 1 gives a yield pressure value of
67.2MPa. This is in good agreement with the numerical value of 68.5MPa.

## 2.2   Optimisation Analysis

## 2.2.1   Theory

In the design of rocket motor cases it is a requirement that the structure
is manufactured to its optimum strength configuration. For overwound
motor cases this configuration will clearly be a function of the pre-
strain induced during winding, the motor rigidity resulting from the
number of applied fibre layers and the mechanical properties of the
constituent materials. A previous analysis (Ref 2) has shown that there

exists a maximum first yield pressure which is independent of the winding strain, the number of applied fibre layers and the physical properties of the fibre.

For the von Mises yield criterion this maximum is given by Equation 14. The maximum is independent of $\varepsilon_w$ and n, (see Ref 2) but the number of layers required to achieve it is inversely related to the winding strain, and vice versa. For a particular motor (Ref 2) this trend is depicted by the dotted line in Figure 2. For the von Mises yield criterion the optimum n values for a prescribed winding strain $\varepsilon_w$, and vice versa, is obtained (Ref 2) as the solution to the equation

$$\left\{ \frac{4R^2}{R^2-R_e^2} -1+An(2\nu_c-1) \right\} \frac{1}{1+An} = \frac{\sqrt{3}\varepsilon_w E_c AF_1(A,n)}{\sigma_y}$$

(25)

For a prescribed n value Equation 25 can be easily solved for the optimum winding strain, but the determination of the optimum number of fibre layers for a prescribed winding strain would generally require computer assistance. This problem can be resolved, however, if Equation 25 is used as the basis for an optimisation nomogram.

As in Section 2.1.1, Equation 25 can be simplified if a non-dimensional approach is adopted. Using Equations 7 to 16, Equation 25 modifies to:

$$\left\{ \frac{4}{\lambda} -1- \frac{\beta}{3} \right\} \frac{1}{1+\beta} = \sqrt{3}\psi_w \ln(1+\beta)$$

(26)

where, as previously, $\nu_c = 1/3$.

The above equation can now be written more conveniently as

$$f_1(\psi_w) + f_2(\lambda)f_3(\beta) = f_4(\beta)$$

(27)

where

$$f_1(\psi_w) = -\sqrt{3}\psi_w$$

$$f_2(\lambda) = 4/\lambda - 1$$

(28)

$$f_3(\beta) = 1/\{(1+\beta)\ln(1+\beta)\}$$

$$f_4(\beta) = \beta/\{3(1+\beta)\ln(1+\beta)\}$$

The resulting nomogram consists of two graduated straight loci representing $\psi_w$ and $\lambda$, and a graduated $\beta$ locus which takes the form of a curve. The nomogram is depicted in Figure 3 with constructional details omitted.

## 2.2.2   Graphical Design Example

For the purposes of illustration Figure 3 is used to determine the optimum
winding strain for the Table 2 motor in terms of the derived variables $\beta$
and $\lambda$ (see Tab 3). The procedure is as follows:

> a.      Draw a straight line to pass through the values of 1.82
> on the $\beta$ scale and 0.5 on the $\lambda$ scale.

> b.      Determine the $\psi_w$ value (1.26) corresponding to the
> intersection of the a. line and the graduated $\psi_w$ locus.

Once $\psi_w$ has been determined, the optimum winding strain follows from a
rearrangement of Equation 10. In this example Figure 3 gives an optimum
winding strain of $8.4 \times 10^{-3}$. This is in good agreement with the numerical
value of $8.5 \times 10^{-3}$. The maximum yield pressure of 92.0MPa corresponding
to this optimum is calculated from Equation 14. This is 36.9% greater
than the yield pressure calculated in Section 2.1.2.

In the above analysis the optimum winding strain has been derived
theoretically. No attempt has been made to assess whether the case could
support the initial stress without yielding. This can be easily checked
using Figure 4 where the winding limit condition, $\hat{\sigma}_{\theta w} = 1 = \psi_w \ln(1+\beta)$
(see Eqn 11), for the variable ranges given in Table 1 is plotted. If the
resulting ($\psi_w, \beta$) coordinate value lies to the right of the line the
case has deformed plastically during winding and the foregoing analysis
is void. Furthermore, an optimised configuration cannot be achieved, a
condition associated with large throat diameters and small inertia loads.

## 3      VISCOELASTIC ANALYSIS

In the preceding section all modulus terms were linear elastic, and the
effects of fibre viscoelastic relaxation were neglected. As a consequence,
closed-form analytical stress solutions were obtained for the fibres and
case from which the required nomograms were constructed.

For short times, ie directly after winding, recent work has shown that
these equations provide a simple and reliable method for the elastic
stress analysis of overwound rocket motor cases. For longer times,
however, these solutions may be in error. Fibre viscoelastic relaxation
may have a significant effect on the case stress immediately before firing
and, as a result, the first yield pressure. Unfortunately, for all but
the most trivial of examples, numerical methods are required to solve the
resulting viscoelastic equations (Ref 4). Nevertheless, analytical
solutions have been obtained for the fully relaxed viscoelastic condition
(Ref 4). Since these solutions are independent of the detailed nature of
the relaxation spectrum (viscoelastic effects are introduced only through
the long-term fibre relaxation modulus $E_f(\infty)$) the resulting equations are
valid for all viscoelastic problems pertaining to this study.

Nomograms for the fully relaxed condition are therefore developed in this
section. For intermediate times numerical methods (Ref 4) must be
employed.

## 3.1    Yield Initiation Predictions

### 3.1.1    Theory

For rocket motor cases subjected to instantaneous pressure loads held for infinitesimally small periods of time the effects of fibre viscoelastic relaxation on the pressure-induced strains are usually neglected. Hence, the pressurisation analysis reduces to an elastic problem, with the pressure-induced stresses and strains related through the conventional Hookean equations.

Omitting details, and using the notation previously defined, the long-term case stress $\sigma_{\theta cp}^{(n)}(\infty)$ on pressurisation following complete viscoelastic relaxation in the fibre can be deduced from Reference 4.

$$\sigma_{\theta cp}^{(n)}(\infty) = -E_c \epsilon_w A F_1(A,n) \left\{ \frac{A(\infty)n + E_f(\infty)/E_f(0)}{1 + A(\infty)n} \right\}$$

$$+ \frac{pR}{t_c(1+An)} \left\{ 1 + \frac{n \nu_c A}{2} \left( 1 - \frac{R_e^2}{R^2} \right) \right\}$$

$$(29)$$

where

$$A(\infty) = \frac{E_f(\infty) t_f}{E_c t_c}$$

$$(30)$$

As before, it is convenient to non-dimensionalise Equation 29 using Equations 7 to 16 to give

$$\hat{\sigma}_{\theta cp}^{(n)}(\infty) = -\hat{\sigma}_{\theta w}(\infty) + \frac{2\hat{p}}{\sqrt{3}\lambda(1+\beta)} \left\{ 2 + \frac{\beta\lambda}{3} \right\}$$

$$(31)$$

where

$$\hat{\sigma}_{\theta cp}^{(n)}(\infty) = \sigma_{\theta cp}^{(n)}(\infty)/\sigma_y$$

$$(32)$$

$$\hat{\sigma}_{\theta w}(\infty) = \psi_w \ln(1+\beta) \left\{ \frac{1+\beta}{\frac{1}{\alpha}+\beta} \right\}$$

$$(33)$$

$$\alpha = E_f(\infty)/E_f(0)$$

$$(34)$$

and $\phi$ is defined by Equation 20. As before $\nu_c = 1/3$. The corresponding non-dimensional component of axial stress is again given by Equation 18

and since the case remains linear elastic the yield criterion is given, as before, by Equation 19 with the quantity $\hat{\sigma}_{\theta cp}^{(n)}$ appearing in that equation replaced by $\hat{\sigma}_{\theta cp}^{(n)}(\infty)$. Equations 18, 19 and 31 provide the basis for nomogram construction.

Equations 18 and 31 can now be used to eliminate $\hat{\sigma}_{zcp}$ and $\hat{\sigma}_{\theta cp}^{(n)}(\infty)$ respectively from the von Mises yield criterion, Equation 19, in favour of $\hat{p}_y$ in order to predict the pressure for the onset of yield. The resulting equation is:

$$\hat{p}_y{}^2 \frac{4}{3}\{1+\phi^2-\phi\} + \hat{p}_y \frac{2}{\sqrt{3}}\{-2\hat{\sigma}_{\theta w}(\infty)\phi+\hat{\sigma}_{\theta w}(\infty)\}$$

$$+ \hat{\sigma}_{\theta w}(\infty)^2 - 1 = 0$$

(35)

On solution, the positive root for $\hat{p}_y$ is then substituted in Equation 9 to obtain the yield pressure $p_y$.

The graphical representation of Equation 35 now follows as for Equation 22, that is, the variation of $\hat{\sigma}_{\theta w}(\infty)$ with $\phi$ is plotted for various $p_y$ values to give the plot depicted in the central portion of Figure 5.

Since the above analysis has been derived in terms of the variable combinations $\hat{\sigma}_{\theta w}(\infty)$ and $\phi$, it is necessary, as before, to construct additional nomograms so that the required *design* chart can be used in conjunction with the fundamental variables $\psi_w$, $\beta$, $\alpha$ and $\lambda$. Although the graphical determination of $\phi$ readily follows from the Equation 23 nomogram, the graphical determination of the effects of complete fibre relaxation on the case pre-stress, $\hat{\sigma}_{\theta w}(\infty)$, cannot be established from the 'z' type nomogram shown to the left of the central plot in Figure 1, since, when viscoelastic effects are introduced, the case pre-stress becomes a function of both the long- and short-term fibre modulus values (see Eqn 33). Under these conditions, the effects of complete fibre relaxation on $\hat{\sigma}_{\theta w}(\infty)$ may be graphically determined from a 'proportional' type nomogram (Ref 6) of the form

$$\frac{f_1(\alpha,\beta)}{f_2(\beta)} = \frac{f_3(\psi_w)}{f_4(\hat{\sigma}_{\theta w}(\infty))}$$

(36)

where the functions represent

$$f_1(\alpha,\beta) = 1/\alpha + \beta = \gamma$$

$$f_2(\beta) = (1+\beta)\ln(1+\beta)$$

$$f_3(\psi_w) = \psi_w$$

(37)

$$f_4(\hat{\sigma}_{\theta w}(\infty)) = \hat{\sigma}_{\theta w}(\infty)$$

As before, the three independent nomograms can be combined through their common loci. The final design chart is shown in Figure 5 with constructional details omitted.

In contrast to Figure 1 the design process embodied in Figure 5 is now in terms of five fundamental variables $\psi_w$, $\lambda$, $\hat{p}_y$, $\alpha$ and $\beta$. However, the variable $\beta$ is again represented by two of the graduated loci in the design chart. (Furthermore, $\gamma$ is a function of $\beta$.) It follows therefore, as before, that $\beta$ cannot be 'read' directly from the design chart in terms of the variables $\psi_w$, $\hat{p}_y$, $\lambda$ and $\alpha$ and that a trial-and-error solution procedure is again required. Nevertheless, this problem can be resolved if the fully relaxed case pre-stress, $\hat{\sigma}_{\theta w}(\infty)$, is specified together with $\lambda$, $\hat{p}_y$ and $\alpha$ so that the solution procedure follows in a manner similar to that described in Section 2.1.1.

### 3.1.2 Graphical Design Example

To illustrate the use of Figure 5 the fully relaxed viscoelastic yield pressure value is calculated for the Table 2 motor using the derived variables given in Table 3. However, as Figures 1 and 5 are identical, except for the case pre-stress nomogram, only the use of the case pre-stress nomogram will be discussed here. The procedure is as follows:

> a. Using the left-hand side of the nomogram, construct an index line to pass through 1.82 on the $\beta$ scale and 3.82 on the $\gamma$ scale. Mark the intersection of this line with the ungraduated diagonal.

> b. From the intersection established in a. draw a second straight line to cut the $\psi_w$ scale at 0.22. Extend to cut the $\hat{\sigma}_{\theta w}(\infty)$ scale at 0.17. This is the non-dimensional fully relaxed viscoelastic case pre-stress.

> c. Having established $\hat{\sigma}_{\theta w}(\infty)$ use steps b. to d. of Section 2.1.2 to calculate the yield pressure as 62.98MPa. This compares favourably with the numerical value of 62.4MPa.

The effects of viscoelastic relaxation can now be assessed. By comparing the yield pressure values obtained from the elastic and fully relaxed viscoelastic conditions (Figs 1&5) for the Table 2 motor case, ie 67.2MPa and 62.9MPa respectively, it can be seen that the yield pressure has decreased by approximately 6.5%. It should be noted, however, that the yield pressure may not always decrease. As has been reported elsewhere (Ref 4), depending on the initial winding configuration, the yield pressure may increase, decrease or increase to a maximum and then decrease with fibre relaxation. Nevertheless, the maximum attainable yield pressure will always be given by Equation 14.

An insight into which of these three yield pressure trends a motor will exhibit can be obtained from a consideration of the $\hat{\sigma}_{\theta w} - \phi$ grids in Figures 1 and 5. If the relevant point lies to the right of the $\hat{p}_y = 1$ curve in Figure 1 the yield pressure will always decrease with fibre relaxation, whereas the opposite is true if the intersection lies to the

left of the $\hat{p}_y = 1$ curve in Figure 5. But, if the intersection lies to the left of the $\hat{p}_y = 1$ curve in Figure 1 and then lies to the right of the $\hat{p}_y = 1$ curve in Figure 5, the yield pressure will have increased to the maximum and then decreased with fibre relaxation. For design purposes the latter trend is preferable, provided the elastic and fully relaxed viscoelastic yield pressure values are equal. Otherwise, depending upon initial winding conditions, the yield pressure value at either the elastic or the fully relaxed viscoelastic condition may take an unacceptably low value.

## 3.2    Optimisation Analysis

### 3.2.1    Theory

In the preceding section it was shown that the yield pressure depends on fibre relaxation. It follows therefore that the elastic optimisation nomogram (Fig 3) is not valid when viscoelastic relaxation occurs.

This is illustrated in Figure 2, where the first yield pressure values are plotted against the number of applied fibre layers for a particular motor (Ref 4) for the elastic and fully relaxed conditions. It can be seen that fibre relaxation is accompanied by a shifting of the yield pressure curve so that the number of fibre layers required for the fully relaxed optimum configuration is greater than that required for the elastic analysis. Furthermore, for the elastic optimised motor the yield pressure in the fully relaxed condition will be lower than that given by Equation 14.

From a previous viscoelastic analysis (Ref 4) it can be shown, after some manipulation, that when viscoelastic effects are introduced the optimisation equation for the fully relaxed condition becomes

$$\{ \frac{4R^2}{R^2-R_e^2} -1+An(2v_c-1)\} \frac{1}{1+An} = \frac{\sqrt{3}\epsilon_w E_c AF_1(A,n)}{\sigma_y} \{\frac{1+An}{\frac{E_f(0)}{E_f(\infty)} +An} \}$$

(38)

For a prescribed number of fibre layers Equation 38 can be solved for the fully relaxed optimum winding strain. Conversely, the determination of the optimum number of fibre layers, for a prescribed winding strain, would generally require computer assistance. It is therefore necessary to represent Equation 38 graphically.

Using Equations 7 to 16 and Equations 32 to 34 and setting $v_c = 1/3$, Equation 38 reduces to the following non-dimensional form:

$$\{\frac{4}{\lambda} -1- \frac{\beta}{3}\} \frac{1}{1+\beta} = \sqrt{3}\epsilon_w \ln(1+\beta) \{\frac{1+\beta}{\frac{1}{\alpha}+\beta}\}$$

(39)

which on subsequent rearrangement corresponds to an alignment nomogram (Ref 6) of the form

$$f_1(\alpha) + f_2(\psi_w)f_3(\lambda,\beta) = f_4(\beta) \tag{40}$$

where the functions represent

$$f_1(\alpha) = 1/\alpha$$

$$f_2(\psi_w) = -\psi_w$$

$$f_3(\lambda,\beta) = \{\sqrt{3}(1+\beta)^2 \ln(1+\beta)\}/\{\frac{4}{\lambda}-1-\frac{\beta}{3}\} \tag{41}$$

$$f_4(\beta) = -\beta$$

This is analogous to Equation 27. The resulting nomogram will therefore consist of two graduated parallel loci for $\psi_w$ and $\alpha$ and a series of graduated curved $\beta$ loci, each for a prescribed $\lambda$ value.

In principle the resulting nomogram will graphically represent Equation 39. In practice, however, experience has shown that unacceptable reading errors can occur for extreme variable combinations. To resolve this problem it is necessary to transform the Equation 40 nomogram into an alternative form so that the resulting design chart possesses greater practical utility.

Using determinant theory (Ref 7) and omitting the details it can be shown (see Annex A) that the required nomogram can be obtained from the basic determinant

$$\begin{vmatrix} -1/f_1(\alpha) & 0 & 1 \\ 0 & -1/f_2(\psi_w) & 1 \\ -1/f_4(\beta) & -f_3(\lambda,\beta)/f_4(\beta) & 1 \end{vmatrix} = 0 \tag{42}$$

This corresponds to a nomogram which consists of a locus for $\alpha$ coincident with the x-axis, a locus of $\psi_w$ coincident with the y-axis and a series of $\beta$ curves, each curve representing a unique $\lambda$ value. Furthermore, the $\alpha$ and $\psi_w$ axes are orthogonal. The resulting nomogram is presented in Figure 6 with the constructional details omitted.

Alternative transformations of Equation 40 can be derived leading to different determinant forms, but these have not led to significantly better nomographic representations.

### 3.2.2 Graphical Design Example

For the purposes of illustration, Figure 6 is used to determine the winding strain necessary to obtain the optimised configuration at the fully relaxed condition for the Table 2 motor in terms of the derived variables given in Table 3. The procedure is as follows:

    a.    Locate a point within the $\lambda - \beta$ grid corresponding to the intersection of $\beta = 1.82$ and $\lambda = 0.5$.

    b.    From this point draw a straight line to pass through 0.5 on the $\alpha$ scale to obtain the required $\psi_w$ value.

For the example considered, Figure 6 gives a winding strain of $1.17 \times 10^{-2}$, as compared to the numerical value of $1.15 \times 10^{-2}$. These values are in good agreement. If the elastic and fully relaxed viscoelastic optimum winding strains are compared ($8.46 \times 10^{-3}$ and $1.17 \times 10^{-2}$ respectively) it can be seen that the latter is 38.3% greater than the former. Consequently, it may not be possible to obtain a fully relaxed optimised configuration; the pre-stress induced during winding may exceed the elastic limits of the case material. This condition can, as previously, be easily checked using Figure 4. If the relevant point lies to the right of the winding limit condition line, ie $\hat{\sigma}_{\theta w} = 1 - \psi_w \ln(1+\beta)$ (see Eqn 11), the case has deformed plastically during winding and the foregoing analysis is void.

## 4     MAXIMUM FIBRE STRESS

### 4.1     Theory

In the foregoing sections, graphical design procedures were developed to determine the maximum permissible applied pressure and the optimised winding configuration for both the initial elastic and fully relaxed conditions. In these analyses the maximum pressure calculation has been based on the pressure for first yield in the case material, and the magnitude of the fibre stresses associated with this pressure has not been studied. In the present application it is likely that this approach will provide a satisfactory design solution, since the ultimate tensile strength of the fibre overwind is very much greater than the yield stress of the case. Nevertheless, care must be taken at the exploratory stages of the design to ensure that the fibre stresses do not exceed prescribed safety values.

A previous study (Ref 2) has shown that the maximum fibre stress occurs in the outermost fibre layer directly after winding. It follows therefore from Equation 1 that the maximum fibre stress $\sigma_{\theta f max}$ is given approximately by

$$\sigma_{\theta f max} = \epsilon_w E_f \{1 - \frac{A}{1+An}\} + \frac{pRA}{t_f(1+An)} \{1 - \frac{1}{6}(1 - \frac{R_e^2}{R^2})\}$$

(43)

where, as previously, $\nu_c = 1/3$. It should be noted that the above equation is also valid for the viscoelastic fibre with $E_f$ replaced by $E_f(0)$.

Again it is convenient to adopt a non-dimensional approach. Using Equations 7 to 16 it can be shown that Equation 43 reduces to:

$$\hat{\sigma}_{\theta f max} = \delta\{\psi_w + \frac{2\hat{p}}{\sqrt{3}(1+\beta)} \{\frac{2}{\lambda} - \frac{1}{3}\}\}$$

(44)

where $\delta$ denotes the modulus ratio $E_f/E_c$ and $\hat{\sigma}_{\theta f max}$ is the non-dimensional maximum fibre stress $\sigma_{\theta f max}/\sigma_y$. In Equation 44 the approximation

$$1 - \frac{A}{1+An} \div 1$$

(45)

has been used.

One of the most simple techniques (Ref 7) for dealing with equations of the above form is to introduce an additional auxiliary variable as follows.

$$\hat{\sigma}_{\theta f max} = \delta\{\psi_w + \kappa\}$$

(46)

where

$$\kappa = \frac{2}{\sqrt{3}} \frac{\hat{p}}{(1+\beta)} \{\frac{2}{\lambda} - \frac{1}{3}\}$$

(47)

Both of these equations can now be readily represented by grid nomograms, Equation 46 by an alignment (Ref 6) nomogram and Equation 47 by a '7' type (Ref 6) nomogram. The complete nomogram is then obtained by combining these two independent nomograms in such a way that the locus $\kappa$ is common to both. It should be noted, however, that if a conventional construction technique is used for the Equation 46 nomogram, the desired grid will not be obtained, since the effect of varying $\lambda$ is merely to adjust the gradations on the $\beta$ scale, not to alter its spatial position relative to the nomogram as a whole. Nevertheless, a pseudo-grid can be constructed whereby the $\beta$ scales, for each unique $\lambda$ value, are projected horizontally onto a pseudo-scale set off to the right-hand side of the actual $\beta$ locus. By passing loci through common variable values on these scales the required grid is formed. The ordinate of any point in the grid is therefore projected horizontally across to the locus which forms the left hand edge of the $\beta$-$\lambda$ grid. This process can, for a known intersection of the left-hand edge of the $\beta$-$\lambda$ grid, be reversed if necessary to obtain $\lambda$ for a known $\beta$, and vice versa.

17

The complete nomogram is depicted in Figure 7 with constructional details omitted. The common locus $\kappa$ is represented by the ungraduated locus located at the centre of the nomogram.

## 4.2    Graphical Design Example

For the purposes of illustration the maximum fibre stress is calculated for the Table 2 motor using the derived variables given in Table 3. The applied internal pressure is taken as that for first yield in the case material assuming elastic conditions (see Section 2.1.2). The procedure is as follows:

   a.    Using the right-hand side of the nomogram determine the intersection of the $\lambda = 0.5$ and $\beta = 1.82$, interpolating as necessary. Project the ordinate of this point horizontally to intersect the left-hand edge of the $\beta$-$\lambda$ grid.

   b.    Construct an index line to pass through the final intersection obtained in a. and the value 0.73 on the $\hat{p}$ scale to cut the locus positioned at the centre of the nomogram.

   c.    Construct a second index line, this time to pass through the grid point corresponding to $\delta = 1.77$ and $\psi_w = 0.22$ and the intersection of the $\kappa$ locus determined in b. to obtain the required $\hat{\sigma}_{\theta fmax}$.

The maximum fibre stress of 1100MPa then follows from the simple relationship $\sigma_{\theta fmax} = \hat{\sigma}_{\theta fmax} \times \sigma_y$. This is in good agreement with the numerical value of 1069MPa and consistent with the approximations made in Equation 44. The UTS of the fibre used in this example (Tab 2) is 2400MPa.

## 5    CONCLUSIONS

Charts have been presented for use in the design of a metallic cylinder reinforced with a viscoelastic fibre overwind. Topics considered include:

   a.    Determination of the pressure for first yield in the metallic case at short- and long-times.

   b.    Determination of the optimised configuration for short- and long-times.

   c.    Determination of the maximum fibre stress.

Examples have been given with each nomogram for a particular component; derived results compare favourably with exact numerical results.

6    REFERENCES

1    Groves A          Stress Analysis of Fibre-Reinforced Metallic
     Margetson J       Rocket-Motor Cases, Unpublished MOD(PE) Report
     Stanley P

2    Stanley P         Analytical Stress Solutions for Fibre-Reinforced
     Margetson J       Metallic Rocket-Motor Cases, Int J mech Sci, 26,
     Groves A          No 2, 1984, pp119-130

3    Margetson J       Stress Analysis Procedures for the Design of
                       Fibre-Reinforced Metallic Rocket Motor Cases.
                       Paper AIAA-83-1330, AIAA/SAE/ASME 19th Joint
                       Propulsion Conference, Seattle, Washington,
                       June 1983

4    Margetson J       Stress Analysis of Metallic Rocket-Motor Cases
     Groves A          Reinforced with a Viscoelastic Fibre Overwind,
     Stanley P         Accepted for publication in Int J mech Sci, 1985

5    Timoshenko S      Theory of Elasticity, 3rd Edn, McGraw-Hill,
     Goodier J N       New York, 1970

6    Levens A S        Nomography, 2nd Edn, John Wiley & Sons Inc,
                       New York, 1948

7    Allcock H J       The Nomogram, 4th Edn, Sir Isaac Pitman & Sons Ltd,
     Jones J R         London, 1950
     Michel J G L

Reports quoted are not necessarily available to members
of the public or to commercial organisations.

7    NOMENCLATURE

**Variables**

| | |
|---|---|
| $A, A(\infty)$ | defined by Equations 3 and 30 respectively |
| $E, E(\infty)$ | short- and long-term Young's modulus values respectively |
| $F_i(A,n)$ | defined by Equation 4 |
| $n$ | number of fibre layers |
| $p$ | internal pressure |
| $R, R_e$ | internal case radius and effective nozzle radius respectively |
| $t$ | thickness |
| $\epsilon$ | strain |
| $\nu$ | Poisson's ratio |
| $\sigma$ | stress |

**Derived Variables**

| | |
|---|---|
| $\hat{p}$ | applied/maximum pressure ratio (see Eqn 9) |
| $\alpha$ | fibre viscoelastic modulus parameter (see Eqn 34) |
| $\beta$ | stiffness parameter (see Eqn 7) |
| $\gamma$ | stiffness-fibre modulus parameter (see Eqn 37) |
| $\delta$ | constituent materials modulus ratio $E_f/E_c$ |
| $\kappa$ | auxiliary variable (see Eqn 47) |
| $\lambda$ | radius parameter (see Eqn 8) |
| $\phi$ | auxiliary variable (see Eqn 20) |
| $\psi_w$ | non-dimensional winding parameter (see Eqn 10) |

**Subscript**

| | |
|---|---|
| $f,c$ | fibre and case respectively |
| max | maximum |
| opt | optimum |
| $p$ | due to pressurisation |
| uts | ultimate tensile strength |
| w | winding |
| y | at first yield |
| $\theta, z$ | circumferential and axial directions respectively |

**Superscript**

| | |
|---|---|
| $(i,n)$ | i'th fibre of n fibre layers |
| $(n)$ | n fibre layers |

**Accent**

| | |
|---|---|
| $\wedge$ | non-dimensional |

TABLE 1    Typical Ranges of Non-Dimensional Variables

| | | Values Min | Max |
|---|---|---|---|
| Non-dimensional winding parameter | $\psi_w$ | 0 | 1.5 |
| "                    case pre-stress | $\hat{\sigma}_{\theta w}$ | 0 | 1.0 |
| Applied/maximum pressure ratio | $\hat{p}$ | 0 | 1.0 |
| Radius parameter | $\lambda$ | 0 | 1.0 |
| Stiffness parameter | $\beta$ | 0 | 5.0 |
| Fibre viscoelastic modulus ratio | $\alpha$ | 0 | 1.0 |
| Stiffness-fibre modulus parameter | $\gamma$ | 0 | 15.0 |
| Constituent materials modulus ratio | $\delta$ | 0 | 4.0 |
| Non-dimensional maximum fibre stress | $\hat{\sigma}_{\theta f max}$ | 0 | 15.0 |

TABLE 2    Sample Motor Case Details

| | | | |
|---|---|---|---|
| Fibre moduli | Short term | $E_f(0)$ | 124GPa |
| | Long term | $E_f(\infty)$ | 62GPa |
| Fibre UTS | | $\sigma_{uts}$ | 2400MPa |
| Case Young's modulus | | $E_c$ | 70GPa |
| Case yield stress | | $\sigma_y$ | 470MPa |
| Thicknesses | fibre | $t_f$ | 0.1mm |
| | case | $t_c$ | 1.95mm |
| Radii | Motor | $R$ | 46.0mm |
| | Effective | $R_e$ | 32.53mm |
| Winding strain | | $\epsilon_w$ | $1.5 \times 10^{-3}$ |
| Number of layers | | $n$ | 20 |

TABLE 3    Derived Variables for Table 2 Motor

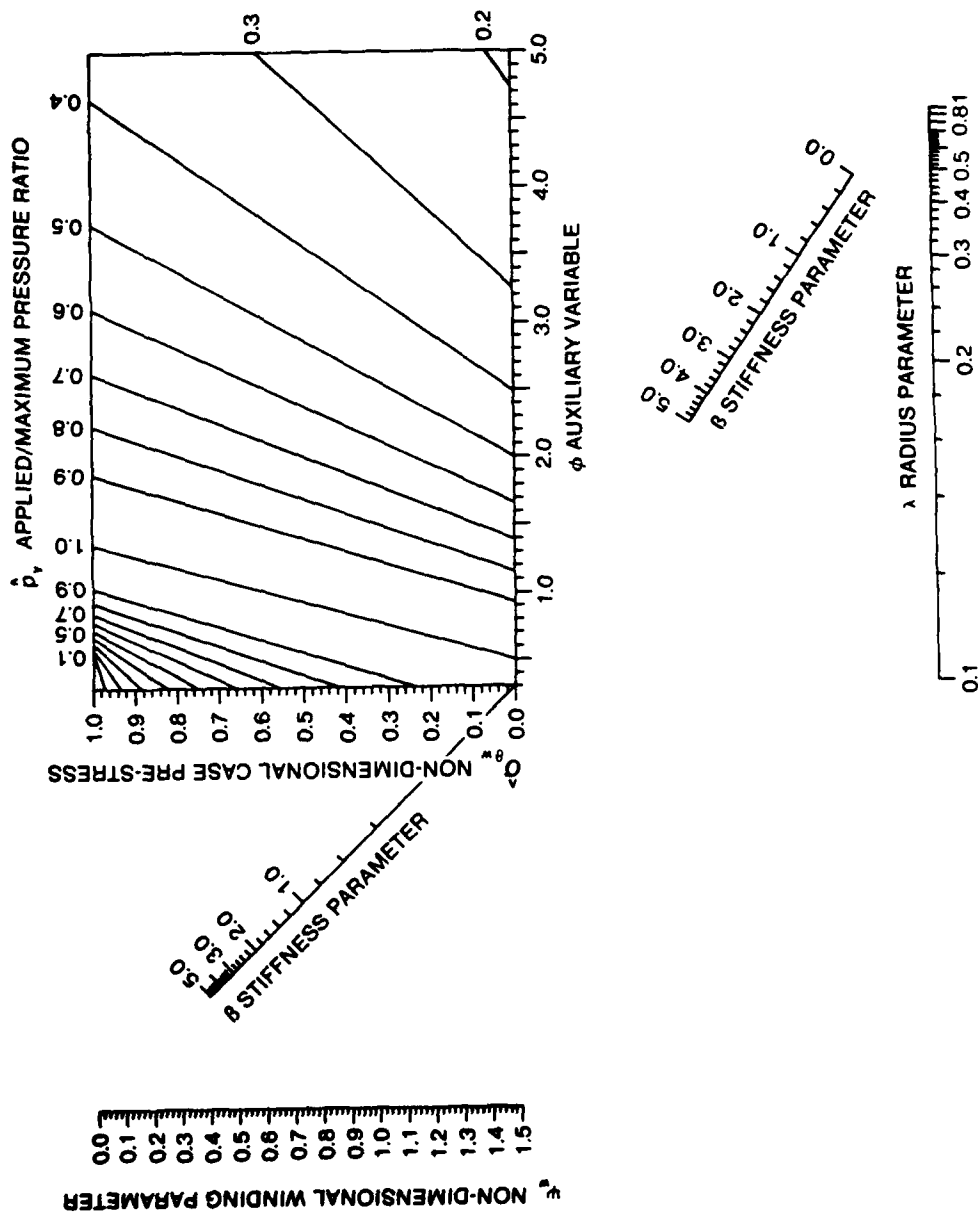| | | |
|---|---|---|
| Non-dimensional winding parameter | $\psi_w$ | 0.22 |
| Radius parameter | $\lambda$ | 0.5 |
| Stiffness parameter | $\beta$ | 1.82 |
| Fibre viscoelastic modulus ratio | $\alpha$ | 0.5 |
| Stiffness-fibre modulus parameter | $\gamma$ | 3.82 |
| Constituent materials ratio | $\delta$ | 1.77 |

FIG. 1



FIG. 1   DESIGN CHART RELATING NON-DIMENSIONAL PRESSURE FOR
ONSET OF YIELD TO DESIGN PARAMETERS: ELASTIC OVERWIND

FIG. 2



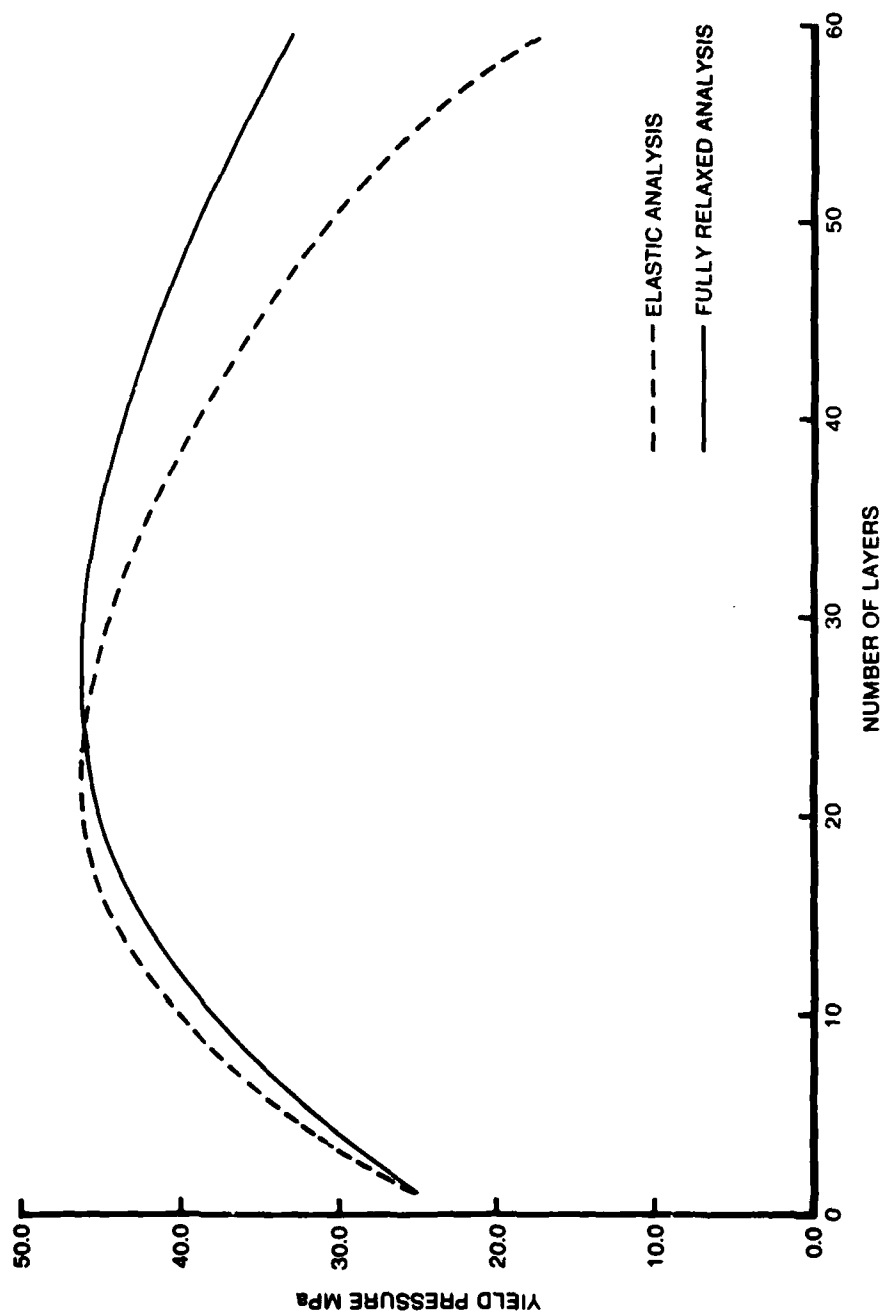FIG. 2   VARIATION OF PRESSURE FOR ONSET OF YIELD WITH NUMBER
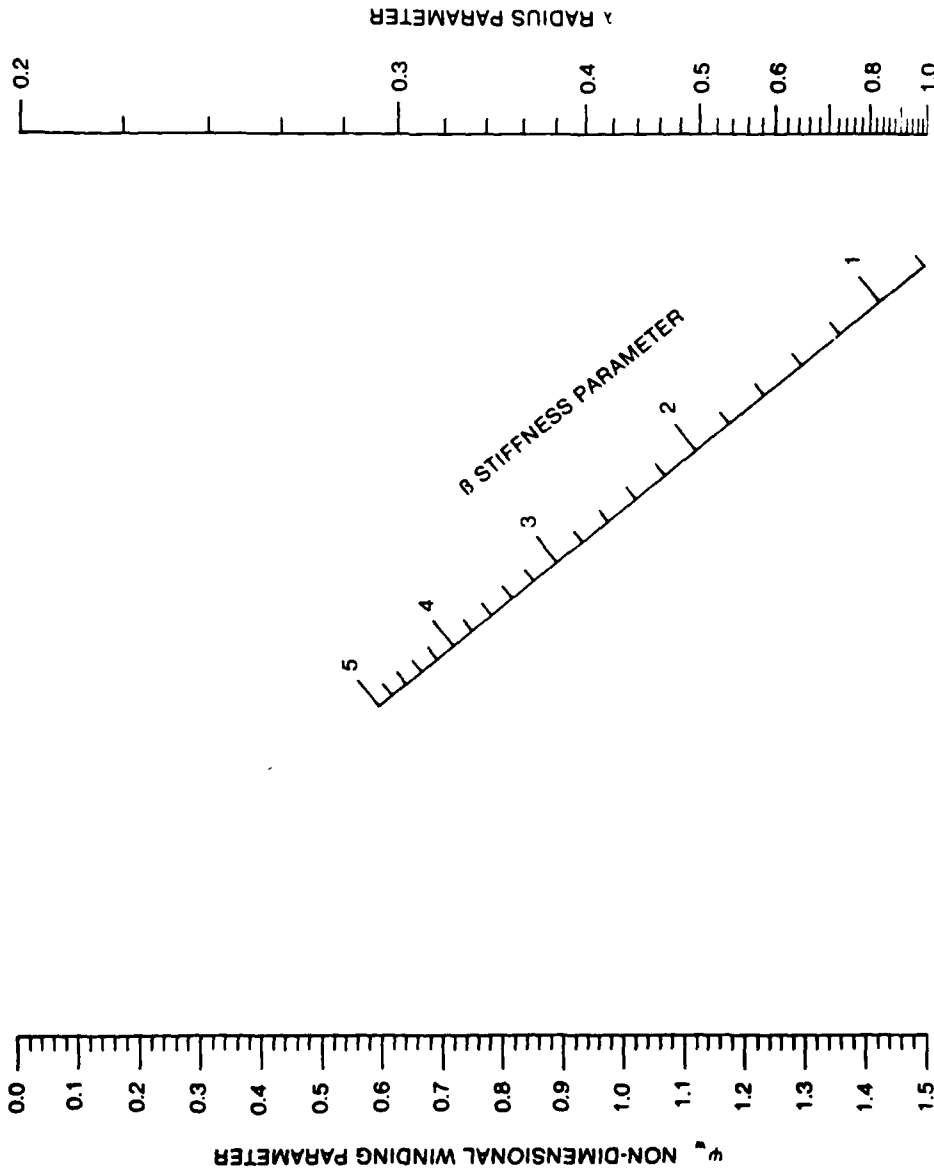OF LAYERS OF REINFORCEMENT

- - - - ELASTIC ANALYSIS

——— FULLY RELAXED ANALYSIS

NUMBER OF LAYERS

YIELD PRESSURE MPa

FIG. 3

λ RADIUS PARAMETER

0.2

0.3

0.4

0.5

0.6

0.8

1.0

β STIFFNESS PARAMETER

5

4

3

2

1

0.0
0.1
0.2
0.3
0.4
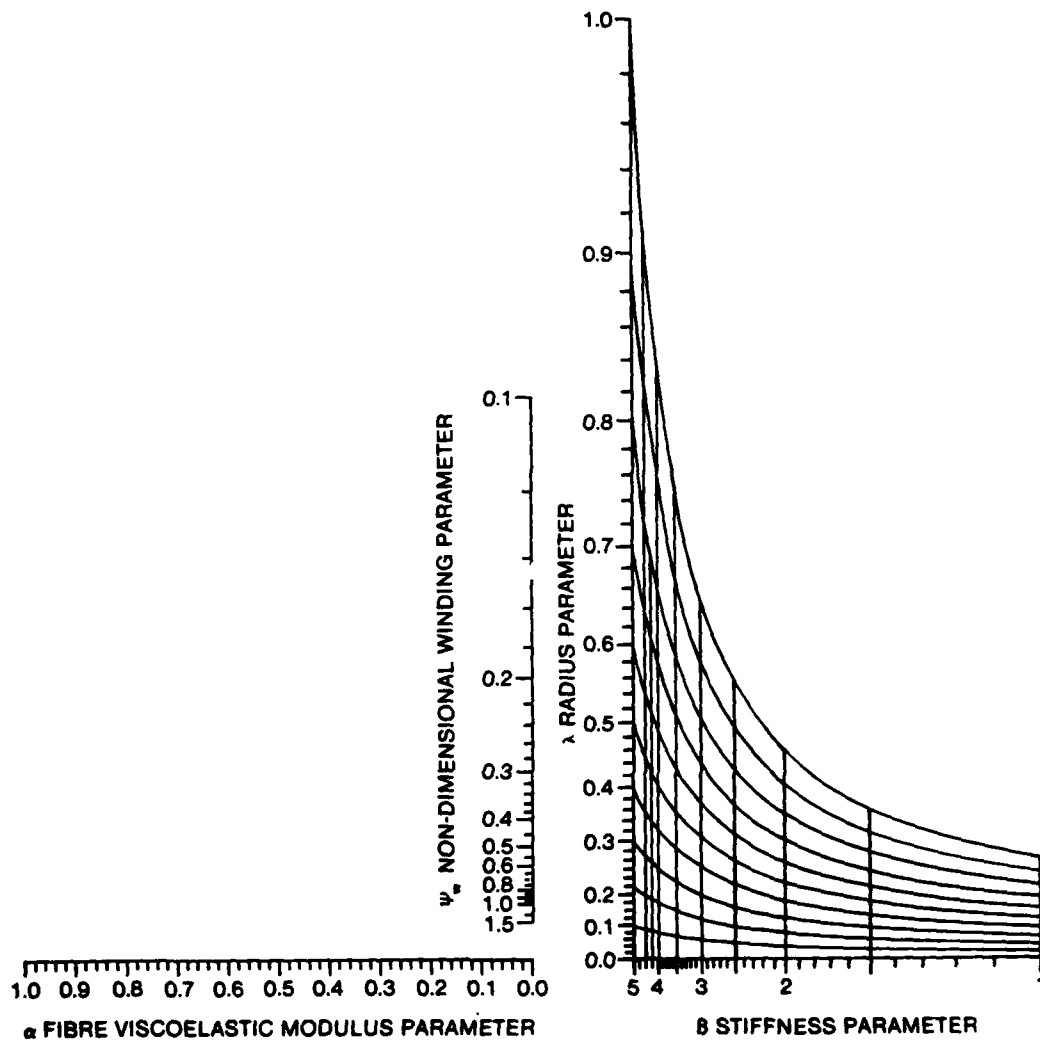0.5
0.6
0.7
0.8
0.9
1.0
1.1
1.2
1.3
1.4
1.5

ψₘ NON-DIMENSIONAL WINDING PARAMETER

FIG. 3    NOMOGRAM RELATING NON-DIMENSIONAL DESIGN PARAMETERS
FOR MAXIMUM FIRST-YIELD PRESSURE: ELASTIC OVERWIND

FIG. 4



ELASTIC DEFORMATION ONLY

β STIFFNESS PARAMETER

ψ_m NON-DIMENSIONAL WINDING PARAMETER
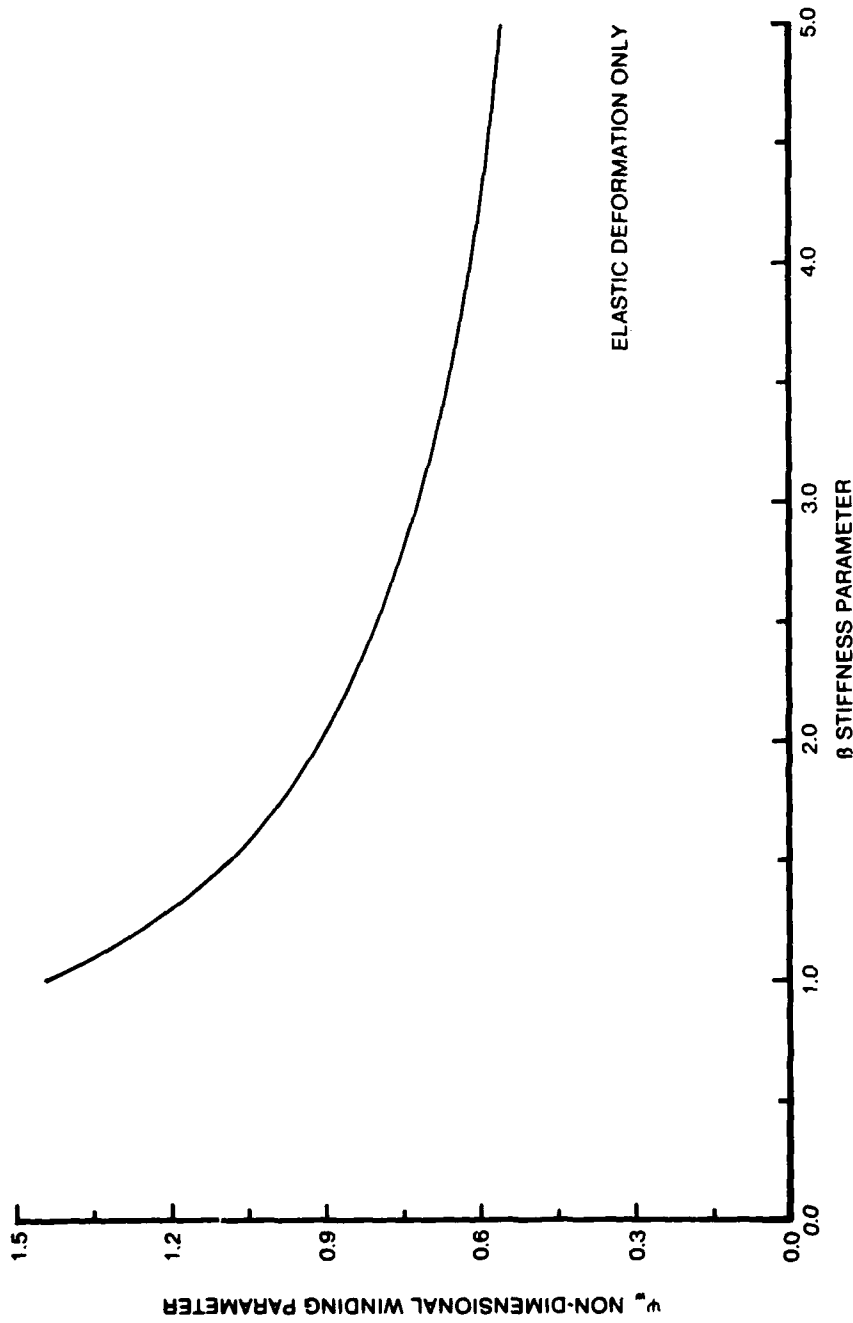
FIG. 4   PLOT OF LIMITING COMBINATIONS OF DESIGN VARIABLES TO
ENSURE ABSENCE OF PLASTIC DEFORMATION DUE TO WINDING
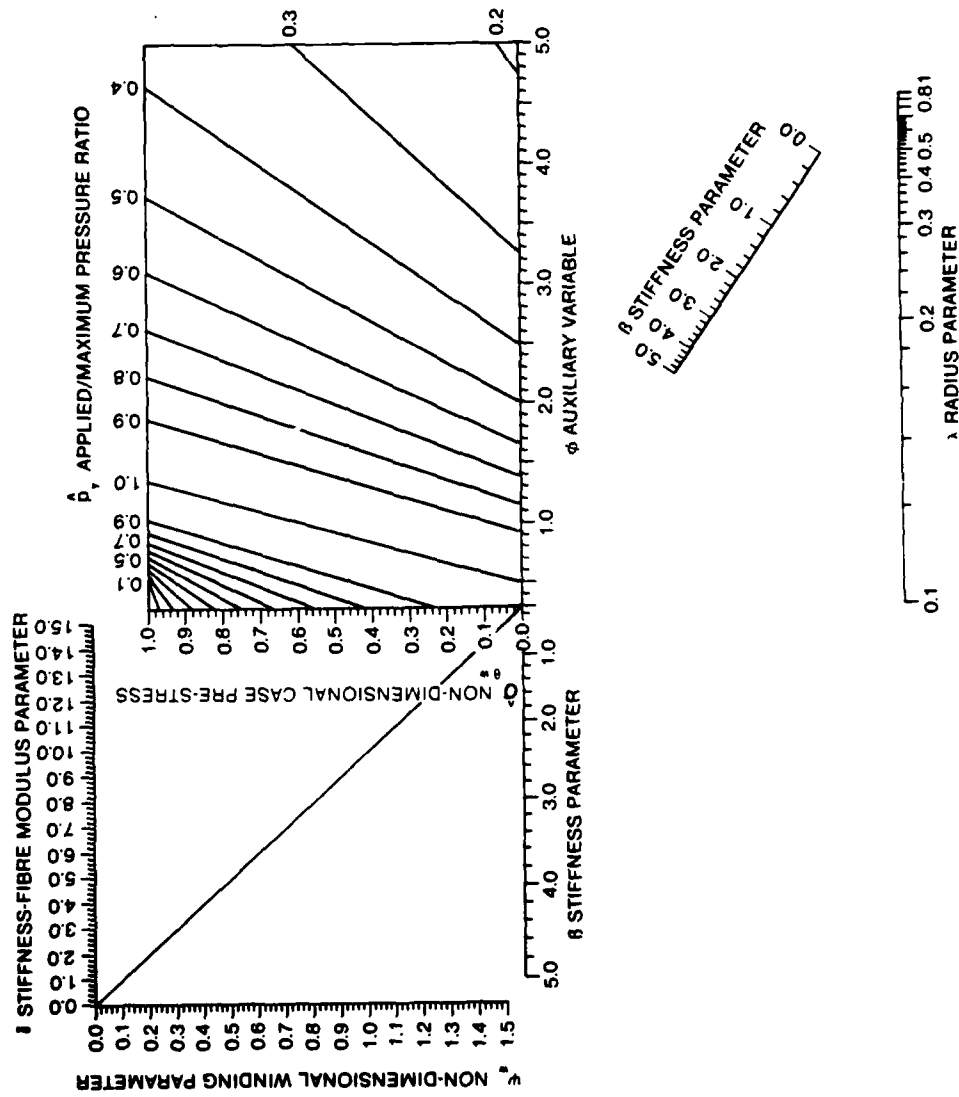
FIG. 5



FIG. 5  DESIGN CHART RELATING NON-DIMENSIONAL PRESSURE FOR ONSET OF
YIELD TO DESIGN VARIABLES: FULLY RELAXED VISCOELASTIC OVERWIND

FIG. 6



**FIG. 6    NOMOGRAM RELATING NON-DIMENSIONAL DESIGN
PARAMETERS FOR MAXIMUM FIRST-YIELD PRESSURE:
FULLY RELAXED VISCOELASTIC OVERWIND**

FIG. 7

λ RADIUS PARAMETER

B STIFFNESS PARAMETER

5 4 3 2 1 0

0.2 0.3 0.4 0.5 0.6 0.7 0.8 0.9 1.0

σ APPLIED/MAXIMUM PRESSURE RATIO

1.0 0.9 0.8 0.7 0.6 0.5 0.4 0.3 0.2 0.1 0.0

ω NON-DIMENSIONAL WINDING PARAMETER

ξ CONSTITUENT MATERIALS MODULUS RATIO

4.0 3.0 2.0 1.0

0.0 0.5 1.0 1.5

σ_f max NON-DIMENSIONAL MAXIMUM FIBRE STRESS

0 1.0 2.0 3.0 4.0 5.0 6.0 7.0 8.0 9.0 10.0 11.0 12.0 13.0 14.0 15.0
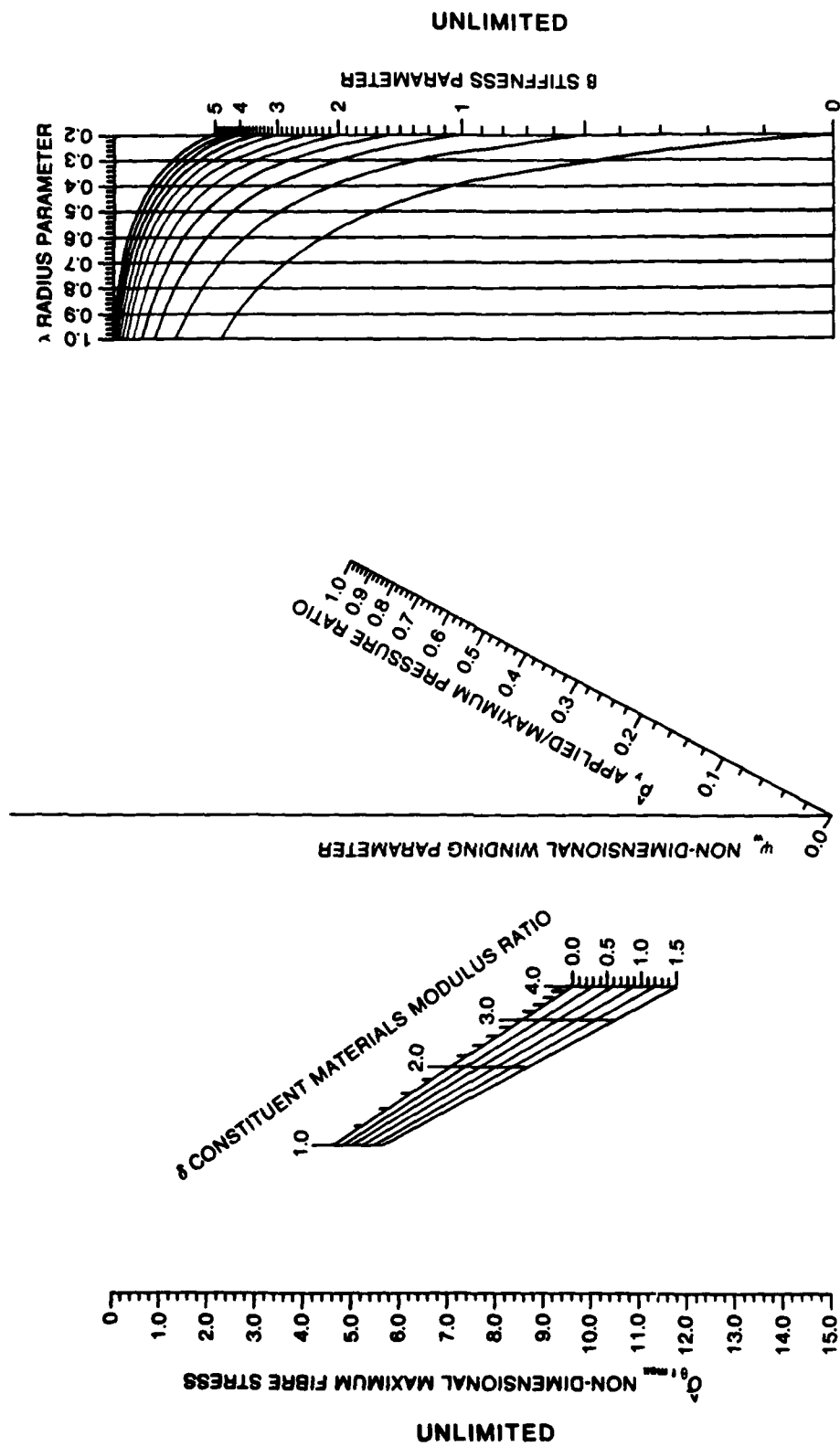
FIG. 7   NOMOGRAM RELATING NON-DIMENSIONAL MAXIMUM FIBRE
STRESS TO NON-DIMENSIONAL DESIGN PARAMETERS

## DETERMINANT THEORY FOR NOMOGRAM CONSTRUCTION

If the coordinate point $x_1, y_1$ is represented parametrically in terms of a, ie

$$x_1 = x_1(a) \qquad y_1 = y_1(a)$$

(A1)

a curve is defined in the x-y plane. Furthermore, if a is specified the corresponding point on the curve is determined. Consequently the curve can be graduated in terms of the parameter a.

Similarly, two further curves can be defined parametrically by the equations

$$x_2 = x_2(b) \qquad y_2 = y_2(b)$$

(A2)

$$x_3 = x_3(c) \qquad y_3 = y_3(c)$$

(A3)

and graduated in terms of the parameters b and c respectively.

If the three coordinate points $x_1,y_1$, $x_2,y_2$ and $x_3,y_3$ are to be co-linear it is a requirement that the gradient of the line joining $x_1,y_1$ and $x_2,y_2$ is the same as that of the line joining $x_1,y_1$ and $x_3,y_3$ ie

$$\frac{y_2-y_1}{x_2-x_1} = \frac{y_3-y_1}{x_3-x_1}$$

(A4)

which, on expanding, and using the parametric relationships defined above gives

$$x_1(a)\{y_2(b)-y_3(c)\} + x_2(b)\{y_3(c)-y_1(a)\} + x_3(c)\{y_1(a)-y_2(b)\} = 0$$

(A5)

This equation can also be expressed in determinant form (Ref 7) as

$$\begin{vmatrix} x_1(a) & y_1(a) & 1 \\ x_2(b) & y_2(b) & 1 \\ x_3(c) & y_3(c) & 1 \end{vmatrix} = 0$$

(A6)

The characteristics of the determinant in Equation A6 are:

a.  its value is zero,
b.  each row contains one parameter only,
c.  each element in the last row is equal to unity.

It is now necessary to regard the parameters a, b and c in Equation A6
as the variables of a three-variable equation. If (and only if) such an
equation can be reduced to a determinant of the form of Equation A6, it
follows that a solution to the equation can be obtained from the points
of intersection of any straight line with the three graduated curves
given by Equations A1, A2 and A3, ie a nomogram can be constructed. The
form of the curves in the nomogram is determined by the elements of the
corresponding row in the determinant (Ref 7).

If, in Equation 40, $f(\alpha)$ is represented by x and $f_2(\psi_w)$ by y, then the
following three simultaneous equations may be written

$$x = f_1(\alpha)$$

$$y = f_2(\psi_w)$$

$$x + f_3(\lambda, \beta)y = f_4(\beta) \tag{A7}$$

ie

$$x + 0y - f_1(\alpha) = 0$$

$$0x + y - f_2(\psi_w) = 0$$

$$x + f_3(\lambda, \beta)y - f_4(\beta) = 0 \tag{A8}$$

The condition for a non-trivial solution of Equation A8 is

$$\begin{vmatrix} 1 & 0 & -f_1(\alpha) \\ 0 & 1 & -f_2(\psi_w) \\ 1 & f_3(\lambda, \beta) & -f_4(\beta) \end{vmatrix} = 0 \tag{A9}$$

This determinant is not of the same form as that of Equation A6, but by
applying standard determinant operations (Ref 7), the following transformed
version can be derived

$$\begin{vmatrix} -1/f_1(\alpha) & 0 & 1 \\ 0 & -1/f_2(\psi_w) & 1 \\ -1/f_4(\beta) & -f_3(\lambda, \beta)/f_4(\beta) & 1 \end{vmatrix} = 0 \tag{A10}$$

where $\lambda$ is considered to be a constant. Equations A6 and A10 are now of
the same form. Consequently, it can be concluded that Equation 40 can be
represented nomographically as detailed in the main text following Equation
42.

Further transformations of Equation A10 can also be performed leading to
different determinant forms, but these have not led to significantly better
nomographic representation of Equation 40.

| 1. DRIC Reference (if known) | 2. Originator's Reference<br>Report 10/84 | 3. Agency Reference | 4. Report Security<br>Classification<br>UNLIMITED |
|---|---|---|---|
| 5. Originator's Code<br>(if known)<br>7699000H | 6. Originator (Corporate Author) Name and Location<br>Ministry of Defence<br>Royal Armament Research and Development Establishment | | |
| 5A. Sponsoring Agency's<br>(Code (if known) | 6A. Sponsoring Agency (Contract Authority) Name and Location | | |

**7. Title** Nomographic Design Procedures for Fibre-Reinforced Metallic Rocket-Motor Cases

**7A. Title in Foreign Language (in the case of translation)**

**7B. Presented at (for conference papers). Title, place and date of conference**

| 8. Author 1, Surname, initials<br>Groves, A. | 9A Author 2<br>Margetson, J. | 9B Authors 3, 4...<br>Stanley, P. | 10. Date<br>January 1986 | pp<br>30 | ref<br>7 |
|---|---|---|---|---|---|
| 11. Contract number and Period | | 12. Project | 13& 14 Other References. | | |

**15. Distribution statement**

**Descriptors (or keywords)**

| Rocket engine cases | Metal products | Nomographs | Design criteria |
|---|---|---|---|
| Cylindrical shells | Fiber laminates | Numerical analysis | |
| Metals | Reinforcement (structures) | Stress analysis | |

**Abstract** Nomographic design procedures are developed for a metallic cylinder (eg a rocket motor case) circumferentially reinforced with a pre-strained fibre overwind with viscoelastic properties. Techniques for calculating the pressure for first yield in the metallic case and the optimum winding conditions for both short- and long- times are presented, together with a technique for determining the maximum fibre stress.

Design examples are presented with each nomogram in turn and the graphical results are compared with exact numerical results.

# END

## DATE
## FILMED

# 8-86